First-principles investigation of two-dimensional trichalcogenide and sesquichalcogenide monolayers

L. Debbichi, H. Kim, T. Björkman, O. Eriksson, and S. Lebègue

Phys. Rev. B **93**, 245307 — Published 24 June 2016

DOI: 10.1103/PhysRevB.93.245307

A theoretical investigation of two dimensional trichalcogenide and sesquichalcogenide monolayers.

L. Debbichi,[1,*] H. Kim,[1] T. Björkman,[2] O. Eriksson,[3] and S. Lebègue[4,†]

[1] *Graduate School of Energy, Environment, Water, and Sustainability (EEWS), Korea Advanced Institute of Science and Technology (KAIST), Yuseong-gu, Daejeon 305-701, Korea.*
[2] *Physics/Department of Natural Sciences, Åbo Akademi University, Porthansgatan 3, 20500 Turku, Finland.*
[3] *Department of Physics and Astronomy, Box 516, Uppsala University, SE-751 20 Uppsala, Sweden*
[4] *Laboratoire de Cristallographie, Résonance Magnétique et Modélisations (CRM2), UMR CNRS 7036) Institut Jean Barriol, Université de Lorraine BP 239, Boulevard des Aiguillettes 54506 Vandoeuvre-lès-Nancy,France*

(Dated: May 27, 2016)

We have used density functional theory to investigate the dynamical stability and the electronic structure of several new semiconducting two-dimensional single layers, with chemical compositions such as ABX_3 and A_2X_3. The calculated interlayer binding energies and the absence of imaginary states in the phonon spectra indicates the possibility to isolate them in the form of a single layer. Also, the calculated band edges reveal that some of these two dimensional materials are promising candidates for water splitting applications.

I. INTRODUCTION

The interest in two dimensional materials presenting electronic properties different from the ones of graphene[1–3] has increased enormously over the last past years. Indeed, although graphene possess an extremely high electron mobility, it lacks a finite bandgap, making its use in transistors difficult. Therefore, researchers became interested in other two-dimensional materials, such as transition metal dichalcogenides (TMDs)[4,5], hexagonal boron nitride (h-BN)[4], or phosphorene[6–9], to name a few[10,11]. Because of their reduced dimensionality, they display peculiar properties: for instance the bandgap of a single layer of MoS_2 is direct while it is indirect in its bulk form[12]. At the same time, optical properties are also significantly different when going from the bulk to the single layer limit: due to the lack of screening along one direction, exciton binding energies are usually much larger than in the bulk[13,14].

Although tremendous progress has already been achieved in synthesizing and studying two dimensional compounds, expanding the landscape of known two-dimensional materials is needed in order to have access to a wider range of properties[15]. For instance, it was shown recently that metal phosphorus trichalcogenides (MPX_3)[16–18], In_2Se_3[19,20], and TiS_3[21,22] are very promising materials for some application in optics and electronics.

In this paper, we study the properties of several trichalcogenide and sesquichalcogenide compounds. In particular, we will focus on the dynamical stability and electronic structure of $AlSiTe_3$, $InSiTe_3$, As_2S_3, As_2Se_3, $\beta-As_2Te_3$, $\beta-Al_2Te_3$, and B_2S_3. All these compounds exist already in the form of bulk crystals (see Fig 1), and their structures have been characterized using X-ray diffraction[23], but very little is known about the properties of the corresponding monolayers. Here we aim at getting such an understanding using ab-initio calculations. Our manuscript is organized as follows: in section II, we describe the different computational methods that we have used in our work, while in section III we present our results, followed by conclusion in section IV.

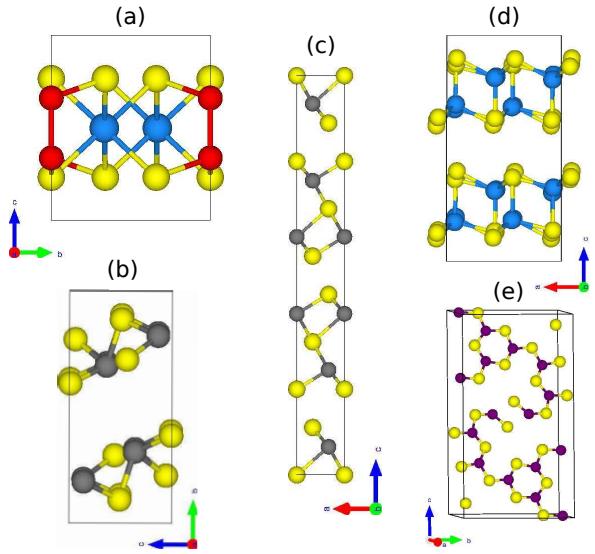

FIG. 1. (color online) Bulk crystal structure of (a) $AlSiTe_3$ (similar for $InSiTe_3$), (b) As_2S_3 (similar for As_2Se_3), (c) β-As_2Te_3 , (d) β-Al_2Te_3, and (e) B_2S_3. The chalcogen atoms (S, Se or Te), Si, Al (In), As, B are represented by yellow, red, blue, gray, and purple spheres, respectively.

II. COMPUTATIONAL DETAILS

The present calculations are based on density functional theory (DFT) and the projector-augmented wave (PAW) method as implemented in the Vienna Ab Initio Simulation Package (VASP)[24]. The Perdew-Burke-

Ernzerhof (PBE)[25] parametrization of the generalized gradient approximation (GGA) is used for the exchange-correlation potential with a plane wave cutoff of 400 eV and a 12 × 12 × 1 and 12 × 7 × 1 k-point mesh for hexagonal and monoclinic structures. Similar parameters were used for the Heyd-Scuseria-Ernzerhof (HSE) calculations[26]. The two dimensional slab geometries were set up with a vacuum space of more than 15 Å to ensure decoupling between periodically repeated systems. Then each system was fully relaxed with residual forces smaller than 0.0001 eV/Å. The dynamical stability of all single layers was determined using the PHONOPY code[27] with 5x5x1 and 6x2x1 supercells for the hexagonal and monoclinic structures respectively, using density functional perturbation theory[28] (DFPT). Interlayer distance and binding energies were calculated with the revB86b-DF2 functional[29] found to give highly consistent values when benchmarked against the random phase approximation[30], and using an in-house implementation[31] of the non-local correlation framework of Dion et al.[32] The interlayer binding energy is then:

$$E_B = \frac{E_{monolayer} - E_{bulk}/N}{A}, \qquad (1)$$

where N is the number of layers in the bulk phase and A is the in-plane area of the monolayer unit cell.

III. RESULTS

The crystal structure and unit cell of the different monolayers investigated here are shown in Fig. 2 (for $AlSiTe_3$, and $InSiTe_3$) and in Fig. 3 (for As_2S_3, As_2Se_3, β-As_2Te_3, β-Al_2Te_3, and B_2S_3).

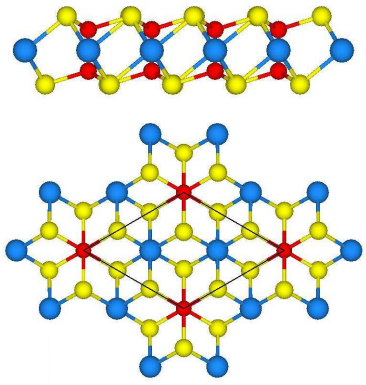

FIG. 2. (color online) Top and side view of a crystal structure of a monoloayer of $AlSiTe_3$ (similar for $InSiTe_3$). The black lines indicate the primitive cell of the system. The chalcogen (Te), Si, and Al are represented by yellow, red, and blue spheres, respectively.

The lattice of the $AlSiTe_3$ and $InSiTe_3$ monolayers is hexagonal, with each silicon atom bonded to one silicon and to three tellurium atoms, while the Al (or In) atoms are at the center of the octahedra formed by the tellurium atoms (see Fig. 2a). Concerning As_2S_3 (and equivalently As_2Se_3), the structure presented in Fig. 3a corresponds to the orpiment phase, having a monoclinic structure with each As atom bonded to three sulfur atoms. The layer is highly corrugated, with sulfur atoms making bonds between As_2S_2 entities. The structure of β-As_2Te_3 differs drastically from its sulfur and selenium counterparts (Fig. 1b): the layer is five atoms thick, with atoms ordered in the sequence Te-As-Te-As-Te in the direction perpendicular to the layer. The structure of β-Al_2Te_3 (see Fig. 3c) is monoclinic, although with a β angle of only 90.04°. The tellurium atoms are at the edge of the monolayer while the aluminum atoms form the core of the material. Notice that the atoms are not positioned on perfectly flat planes and some slight puckering can be observed, which is related to the fact that the cell is not tetragonal but monoclinic. The crystal structure of B_2S_3 is pictured in Fig. 3d. B_2S_3 has a monoclinic lattice ($\beta = 96.23°$) made of chains of S_3 triangles with a boron atom at the center, connected to each other by sulfur atoms. The monolayer is one atom thick, although the layer is not perfectly flat.

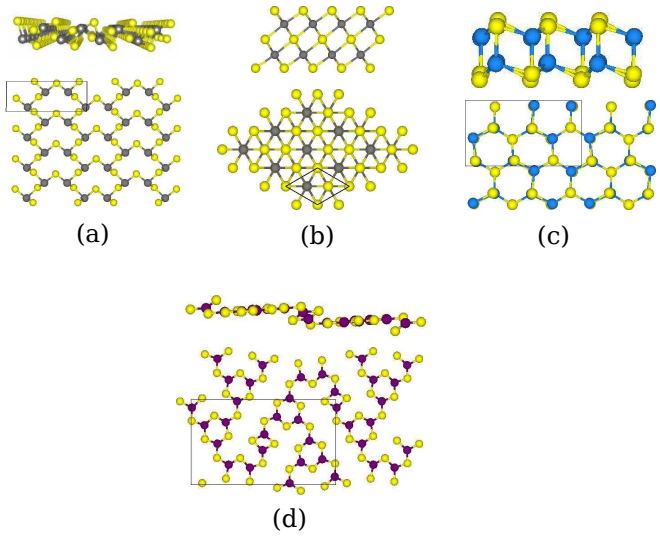

FIG. 3. (color online) Crystal structure of (a) orpiment As_2S_3 (similar for As_2Se_3), (b) β-As_2Te_3 (c) β-Al_2Te_3, and (d) B_2S_3 monolayers: top and side views. The chalcogen atoms (S,Se or Te) are shown in yellow color, and As, Al and B are shown in gray, blue and purpule color, respectively. Black lines indicate the primitive cell of the crystals.

Our calculated binding energies per unit area and interlayer distances, defined as the nearest-neighbor gap between the layers, are presented in Table I. We found that the values fall within the range of values typical of van der Waals bonded solids[33] such as graphite, h-BN, and $MoSe_2$, which suggests these materials as strong candidates for compounds that can exist as free-standing

TABLE I. Interlayer binding energy E_b (in meV/Å^2) and interlayer distances d (defined as the nearest neighbor distance across the gap, in Å) of the various systems investigated here as calculated with the revB86b-DF2 functional[29]. The binding energy and interlayer distances of some well-known layered materials are also shown for comparison.

Stru.	E_b(meV/Å^2)	d(Å)
$AlSiTe_3$	17.6	4.01
$InSiTe_3$	18.3	4.01
As_2S_3	19.9	3.44
As_2Se_3	22.1	3.56
As_2Te_3	24.9	3.62
Al_2Te_3	15.2	4.00
B_2S_3	15.2	3.57
$MoSe_2$[a]	21.6	3.55
h-BN[a]	20.5	3.27
Graphite[a]	21.0	3.62

[a] Ref.[30].

layers[34]. To further strengthen this prediction, we have studied their dynamical stabilities. In Fig. 4 and Fig. 5, we present the calculated phonon dispersion curves of all the compounds (in a monolayer form shown in Figs. 2 and 3) investigated here. No unstable phonon modes are observed in the phonon dispersion curves, confirming the dynamical stability of the 2D form of these materials (in a few cases, there appears to be a weakly unstable phonon branch in a small pocket very close to the Brillouin zone center: this is not a real physical effect, but reflects the well-known difficulty in achieving numerical convergence for the flexural phonon mode for 2D materials[35]).

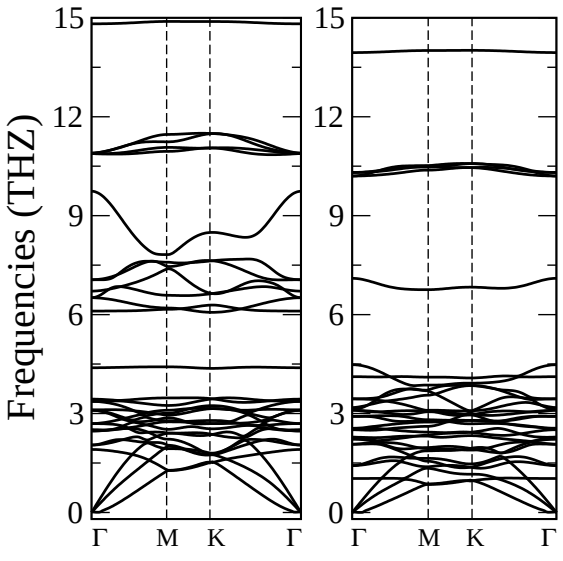

FIG. 4. Phonon dispersion curves of $AlSiTe_3$ (left side) and $InSiTe_3$ (right side).

In addition to the dynamical stability of these systems, we have also investigated their electronic properties. From our calculated PBE electronic bandstructures,

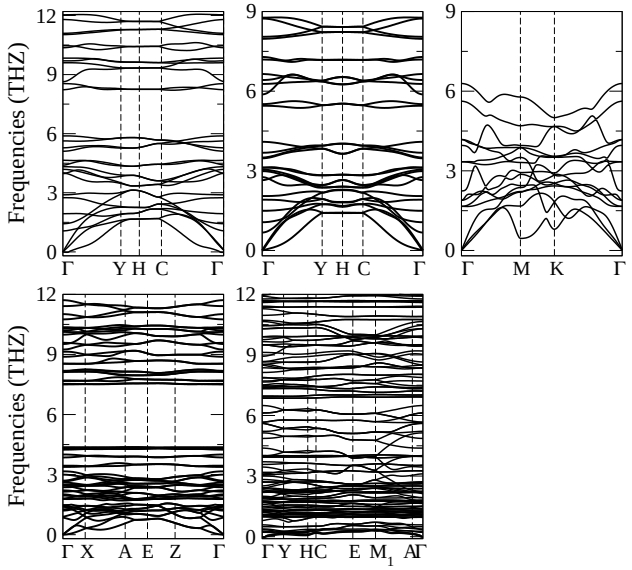

FIG. 5. Phonon dispersion curves from the top to the left side of As_2S_3, As_2Se_3, β-As_2Te_3, β-Al_2Te_3 and B_2S_3 single layers.

TABLE II. Crystal symmetries and calculated electronic bandgap E_g (in eV) of the monolayers investigated here using the PBE and HSE functionals, and the nature of the gap (I: indirect and D: direct gap).

stru.	Sym.	E_g^{PBE}	E_g^{HSE}	Bandgap
$AlSiTe_3$	hex.	1.34	2.05	I
$InSiTe_3$	hex.	0.89	1.54	I
As_2S_3	mon.	2.12	2.95	I
As_2Se_3	mon.	1.64	2.25	I
β-As_2Te_3	rhom.	0.72	1.05	I
β-Al_2Te_3	mon.	1.91	2.61	I
B_2S_3	mon.	2.71	3.79	D

we found that all the monolayers are semiconductors. Considering the fact that the PBE functional usually underestimates the electronic bandgap of semiconducting materials, the HSE06 functional was used to get more realistic values. The obtained bandgaps are shown in the Table II for both PBE and HSE06 functionals together with the nature (direct (D) or indirect (I)) of the gap. The HSE06 bandstructures are shown in figures 6 and 8. The energy gaps are found to be between 1.05 eV and 3.79 eV, in the range of visible light, with B_2S_3 having the largest (3.79 eV) and β-As_2Te_3 having the smallest (1.05 eV) bandgap. Also, we have found that only B_2S_3 has a direct bandgap at the Γ point of the Brillouin zone. Among this list of semiconductors, there are isostructural compounds such as $MSiTe_3$ (M=Al, In) and As_2X_3 (X=S, Se). In the case of $AlSiTe_3$ and $InSiTe_3$, we found that the bandgap decreases from 2.05 to 1.54 eV when changing Al for In, followed by a change of the valence band maximum (VBM) location while the con-

duction band minimum (CBM) is located in the same position (for $AlSiTe_3$ the VBM and CBM are found between M-Γ and K-M, respectively, while in $InSiTe_3$ the VBM and the CBM are found at the K and between K-M high symmetries points). According to the calculated partial density of states (PDOS) shown in Fig. 7, the VBM comes from the chalcogen atoms while the CBM is an hybridization between the Al(In) and the Te atoms. However in the case of As_2X_3 (X=S, Se), we have found that increasing the X atomic number only reduces the band gap by ∼0.7 eV. The PDOS of the M_2X_3 are shown in the Fig 9, we found that for most of these compounds the VBMs belong to the chalcogen atoms while the CBMs belong to the M atoms: only in the case of Al_2Te_3 the VBM and CBM are belonging to the M atoms.

Also, according to our calculated HSE06 bandgap, some of these materials have a suitable bandgap to be used in certain optoelectronics devices: among them, $InSiTe_3$, $AlSiTe_3$, β-Al_2Te_3 and As_2X_3 have a bandgap in the same range as transition metal dichalcogenides[36–38] or phosphorene[39–41].

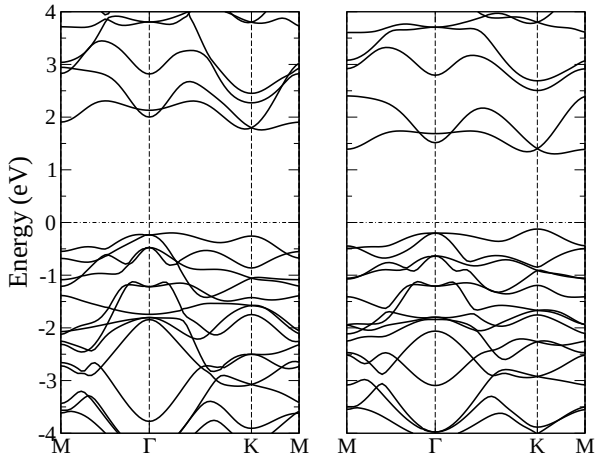

FIG. 6. Calculated electronic bandstructure of $AlSiTe_3$ (left) and $InSiTe_3$ (right) monolayers using the HSE06 functional. States with negative energies correspond to valence states, while states with a positive energy correspond to conduction states.

Furthermore, we have analyzed their electronic structures to investigate whether these compounds could be used for photocatalytic water splitting applications. To be usable for water splitting, a semiconductor is required to have a sizeable bandgap exceeding the free energy of water splitting of 1.23 eV to allows the absorption of a large portion of the solar spectrum[42]. In addition to the magnitude of the bandgap, the band edges must straddle the redox potentials of water so that the reactions are thermodynamically accessible upon optical absorption[43,44]. To verify these properties, the CBM and VBM energy levels obtained by computing the workfunction[45] of each system using the HSE06 functional and compared to water's redox potential are shown

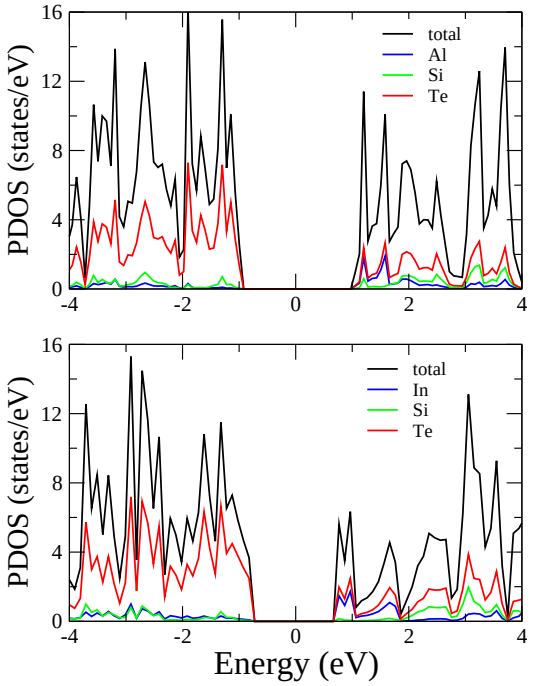

FIG. 7. Total and partial density od states of $AlSiTe_3$ (top) and $InSiTe_3$ (bottom) monolayers. The Fermi level is set at zero level.

in Fig. 10.

It's known that for water splitting reaction, the redox potential is depending on the pH value[46–48]. The standard reduction and oxidation potential with respect to the vacuum level for H^+/H_2 and O_2/H_2O (at pH = 0) are calculated by using the following equation: $E^{red}_{H^+/H_2}$ = -4.44 eV + pH × 0.059 and by $E^{ox}_{O_2/H_2O}$ = -5.67 eV + pH × 0.059 eV, respectively.

As shown in Fig 10, the comparison of the calculated valence band-edge (E_v) and conduction band-edge (E_c) with the redox potential of water at pH = 0, shows that $AlSiTe_3$, $InSiTe_3$, As_2S_3, As_2Se_3 and B_2S_3 layers have their bandgap satisfying the requirement, and their band-edges situated in energetically favorable positions for water splitting.

IV. CONCLUSION

In summary, we have used first principles calculations to study a set of two-dimensional compounds. Their dynamical stability is demonstrated by the phonon dispersion curves and the study of their electronic bandstructures shows that all of them are semiconductors with a bandgap in the range of visible light. The interlayer binding energy is found to be typical of van der Waals bonding. Also, the calculation of their band edges show that several monolayers are good candidates for photocatalytic hydrogen generation.

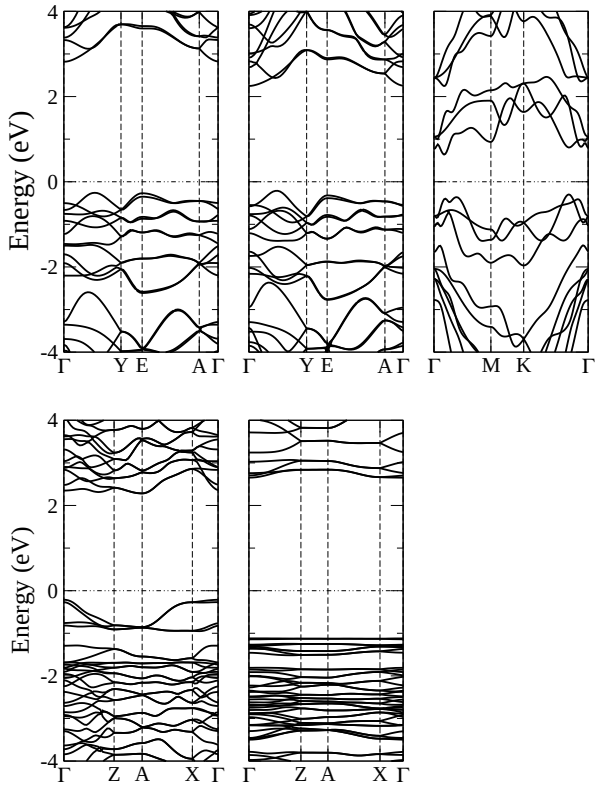

FIG. 8. Calculated electronic bandstructure of M_2X_3 monolayers using the HSE06 functional: from the top to the left As_2S_3, As_2Se_3, β-As_2Te_3, β-Al_2Te_3 and B_2S_3. States with negative energies correspond to valence states, while states with a positive energy correspond to conduction states.

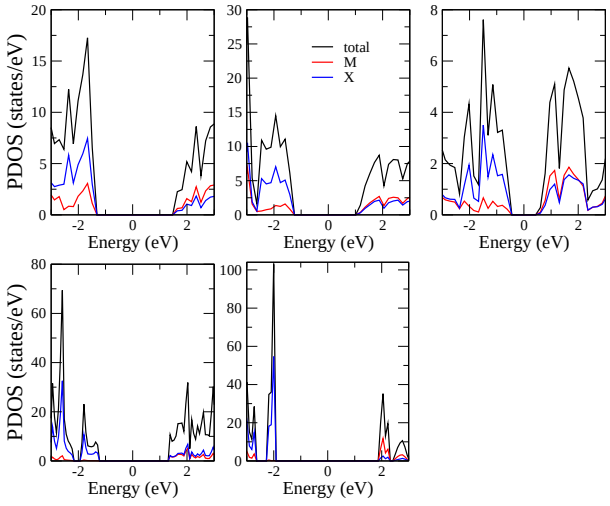

FIG. 9. Total and partial density of states (PDOS) of M_2X_3 monolayers: from the top to the left As_2S_3, As_2Se_3, β-As_2Te_3, β-Al_2Te_3 and B_2S_3. The Fermi level is set at zero level.

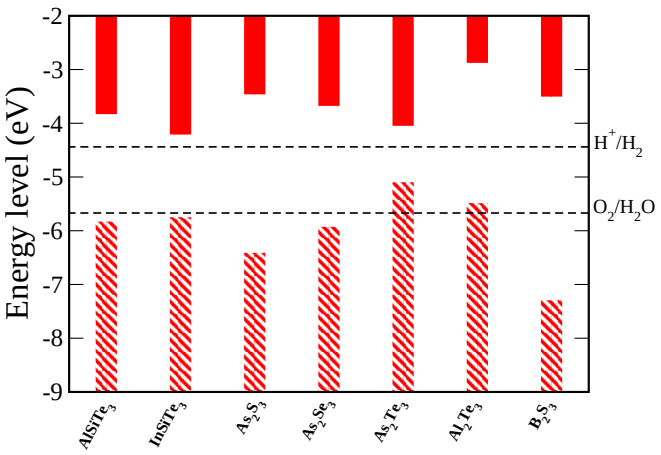

FIG. 10. (color online) Band-edges of the semiconducting trichalcogenide single layers obtained with HSE06, with reference to the water redox potential. Valence and conductions band-edges are shown with green and red color, respectively and the dotted lines indicate the water reduction (H^+/H_2) and oxidation (H_2O/O2) potentials at pH = 0.

ACKNOWLEDGMENTS

The authors acknowledge DARPA and Navy-NICOP for funding. O. E. gratefully acknowledges the Swedish Research Council (VR), SSF, and the Knut and Alice Wallenberg Foundation for financial support. O. E. also acknowledges eSSENCE and STANDUPP. This work was performed using HPC resources from GENCI-CCRT/CINES (Grant x2016-085106). L. D. and H. K. acknowledge the support by the Global Frontier R&D Program (2013M3A6B1078884) on Center for Hybrid Interface Materials (HIM) funded by the Ministry of Science, ICT & Future Planning. T.B. gratefully acknowledges computational resources provided by Finlands IT Centre for Science (CSC)

* debbichi@kaist.ac.kr
† sebastien.lebegue@univ-lorraine.fr

[1] K. S. Novoselov, A. K. Geim, S. V. Morozov, D. Jiang, Y. Zhang, S. V. Dubonos, I. V. Grigorieva, and A. A. Firsov, Science **306**, 666 (2004).
[2] A. K. Geim and K. S. Novoselov, Nature Materials **6**, 183 (2007).
[3] G. W. Flynn, The Journal of Chemical Physics **135**, 050901 (2011).
[4] K. S. Novoselov, D. Jiang, F. Schedin, T. J. Booth, V. V. Khotkevich, S. V. Morozov, and A. K. Geim, Proceedings of the National Academy of Sciences of the United States of America **102**, 10451 (2005).
[5] J. N. Coleman, M. Lotya, A. ONeill, S. D. Bergin, P. J. King, U. Khan, K. Young, A. Gaucher, S. De, R. J. Smith, I. V. Shvets, S. K. Arora, G. Stanton, H.-Y. Kim, K. Lee, G. T. Kim, G. S. Duesberg, T. Hallam, J. J. Boland, J. J. Wang, J. F. Donegan, J. C. Grunlan, G. Moriarty, A. Shmeliov, R. J. Nicholls, J. M. Perkins, E. M. Grieveson, K. Theuwissen, D. W. McComb, P. D. Nellist, and V. Nicolosi, Science **331**, 568 (2011).
[6] F. Xia, H. Wang, and Y. Jia, Nature Communications **5** (2014), 10.1038/ncomms5458.
[7] L. Li, Y. Yu, G. J. Ye, Q. Ge, X. Ou, H. Wu, D. Feng, X. H. Chen, and Y. Zhang, Nature Nanotechnology **9**, 372 (2014).
[8] H. Liu, A. T. Neal, Z. Zhu, Z. Luo, X. Xu, D. Tomnek, and P. D. Ye, ACS Nano **8**, 4033 (2014).
[9] S. P. Koenig, R. A. Doganov, H. Schmidt, A. H. C. Neto, and B. zyilmaz, Applied Physics Letters **104**, 103106 (2014).
[10] A. K. Geim and I. V. Grigorieva, Nature **499**, 419 (2013).
[11] M. Xu, T. Liang, M. Shi, and H. Chen, Chemical Reviews (2013), 10.1021/cr300263a.
[12] S. Lebègue and O. Eriksson, Phys. Rev. B **79**, 115409 (2009).
[13] A. Ramasubramaniam, Physical Review B **86**, 115409 (2012).
[14] M. M. Ugeda, A. J. Bradley, S.-F. Shi, F. H. da Jornada, Y. Zhang, D. Y. Qiu, W. Ruan, S.-K. Mo, Z. Hussain, Z.-X. Shen, F. Wang, S. G. Louie, and M. F. Crommie, Nat Mater **13**, 1091 (2014-12).
[15] S. Lebègue, T. Bjorkman, M. Klintenberg, R. M. Nieminen, and O. Eriksson, Phys. Rev. X **3**, 031002 (2013).
[16] J. Liu, X.-B. Li, D. Wang, W.-M. Lau, P. Peng, and L.-M. Liu, The Journal of Chemical Physics **140**, 054707 (2014).
[17] A. R. Wildes, V. Simonet, E. Ressouche, G. J. McIntyre, M. Avdeev, E. Suard, S. A. J. Kimber, D. Lançon, G. Pepe, B. Moubaraki, and T. J. Hicks, Phys. Rev. B **92**, 224408 (2015).
[18] K. zhao Du, X. zhi Wang, Y. Liu, P. Hu, M. I. B. Utama, C. K. Gan, Q. Xiong, and C. Kloc, ACS Nano **10**, 1738 (2016).
[19] L. Debbichi, O. Eriksson, and S. Lebègue, J.Phys. Chem. Letters **6**, 3098 (2015).
[20] J. Zhou, Q. Zeng, D. Lv, L. Sun, L. Niu, W. Fu, F. Liu, Z. Shen, C. Jin, and Z. Liu, Nano Letters (2015), 10.1021/acs.nanolett.5b01590.
[21] E. Guilmeau, D. Berthebaud, P. R. N. Misse, S. Hbert, O. I. Lebedev, D. Chateigner, C. Martin, and A. Maignan, Chemistry of Materials **26**, 5585 (2014).
[22] J. Dai and X. C. Zeng, Angewandte Chemie International Edition **54**, 7572 (2015).
[23] F. H. Allen, Acta Crystallographica Section B **58**, 380 (2002).
[24] G. Kresse and J. Hafner, Phys. Rev. B **47**, 558 (1993).
[25] J. P. Perdew, K. Burke, and M. Ernzerhof, Phys. Rev. Lett. **78**, 1396 (1997).
[26] J. Heyd, G. E. Scuseria, and M. Ernzerhof, The Journal of Chemical Physics **118**, 8207 (2003).
[27] A. Togo, F. Oba, and I. Tanaka, Phys. Rev. B **78**, 134106 (2008).
[28] X. Gonze and C. Lee, Phys. Rev. B **55**, 10355 (1997).
[29] I. Hamada, Phys. Rev. B **89**, 121103 (2014).
[30] T. Björkman, The Journal of Chemical Physics **141**, 074708 (2014).
[31] A. Gulans, M. J. Puska, and R. M. Nieminen, Phys. Rev. B **79**, 201105 (2009).
[32] M. Dion, H. Rydberg, E. Schröder, D. C. Langreth, and B. I. Lundqvist, Phys. Rev. Lett. **92**, 246401 (2004).
[33] T. Björkman, A. Gulans, A. V. Krasheninnikov, and R. M. Nieminen, Physical Review Letters **108**, 235502 (2012).
[34] B. C. Revard, W. W. Tipton, A. Yesypenko, and R. G. Hennig, Phys. Rev. B **93**, 054117 (2016).
[35] V. Zlyomi, N. D. Drummond, and V. I. Fal'ko, Physical Review B **89**, 205416 (2014).
[36] Q. H. Wang, K. Kalantar-Zadeh, A. Kis, J. N. Coleman, and M. S. Strano, Nature Nanotechnology **7**, 699 (2012).
[37] D. Braga, I. G. Lezama, H. Berger, and A. F. Morpurgo, Nano Letters **12**, 5218 (2012).
[38] J. Kang, S. Tongay, J. Zhou, J. Li, and J. Wu, Applied Physics Letters **102**, 012111 (2013).
[39] H. Liu, A. T. Neal, Z. Zhu, Z. Luo, X. Xu, D. Tomnek, and P. D. Ye, ACS Nano **8**, 4033 (2014).
[40] V. Tran, R. Soklaski, Y. Liang, and L. Yang, Phys. Rev. B **89**, 235319 (2014).
[41] A. Rodin, A. Carvalho, and A. Castro Neto, Physical Review Letters **112**, 176801 (2014).
[42] A. K. Singh, K. Mathew, H. L. Zhuang, and R. G. Hennig, The Journal of Physical Chemistry Letters **6**, 1087 (2015).
[43] Y. Gai, J. Li, S.-S. Li, J.-B. Xia, and S.-H. Wei, Phys. Rev. Lett. **102**, 036402 (2009).
[44] R. Navarro Yerga, M. lvarez Galvn, F. delValle, J. VilloriadelaMano, and J. Fierro, ChemSusChem **2**, 471 (2009).
[45] A. Walsh and C. R. A. Catlow, J. Mater. Chem. **20**, 10438 (2010).
[46] V. Chakrapani, J. C. Angus, A. B. Anderson, S. D. Wolter, B. R. Stoner, and G. U. Sumanasekera, Science **318**, 1424 (2007).
[47] J. Wang, N. Umezawa, and H. Hosono, Advanced Energy Materials **6**, n/a (2016), 1501190.
[48] X. Zhang, X. Zhao, D. Wu, Y. Jing, and Z. Zhou, Advanced Science , 1600062 (2016).